NASA Technical Paper 3105

Influence of Airfoil Geometry on Delta Wing Leading-Edge Vortices and Vortex-Induced Aerodynamics at Supersonic Speeds

Richard M. Wood, James E. Byrd, and Gary F. Wesselmann

March 1992

Contents

Symbols

A	wing planform area, ft^2
c	wing chord, in.
C_N^{l}	normal-force coefficient on wing lower surface, $\dfrac{1}{q_\infty A}\displaystyle\int_{S_A}(p_\alpha - p_{\alpha=0^\circ})\,dx\;dy$
C_N^u	normal-force coefficient on wing upper surface, $\dfrac{1}{q_\infty A}\displaystyle\int_{S_A}(p_\alpha - p_{\alpha=0^\circ})\,dx\;dy$
C_p	pressure coefficient, $\dfrac{p - p_\infty}{q_\infty}$
M	Mach number
M_N	component of Mach number normal to wing leading edge, $M\cos\Lambda(1 + \sin^2\alpha\tan^2\Lambda)^{1/2}$
p	static pressure, lb/ft^2
p_α	static pressure at given angle of attack, lb/ft^2
p_∞	free-stream static pressure, lb/ft^2
q_∞	free-stream dynamic pressure, lb/ft^2
U_∞	free-stream velocity
x, y, z	orthogonal coordinate system referenced to wing apex
α	angle of attack, deg
α_N	angle of attack normal to wing leading edge, $\tan^{-1}\dfrac{\tan\alpha}{\cos\Lambda}$, deg
β	$= \sqrt{M^2 - 1}$
δ_F	wing leading-edge streamwise deflection angle positive when leading edge down, deg
η	fraction of local wing semispan
Λ	wing streamwise leading-edge sweep angle, deg

Abstract

An assessment of the influence of airfoil geometry on delta wing leading-edge vortex flows and vortex-induced aerodynamics at supersonic speeds is made. A series of delta wing wind tunnel models were tested in the Langley Unitary Plan Wind Tunnel over a Mach number range from 1.70 to 2.00. The model geometric variables included leading-edge sweep and airfoil shape. Surface pressure data and vapor-screen and oil-flow photographs were taken to evaluate the complex structure of the vortices and shocks on the family of wings tested. The data show that airfoil shape has a significant impact on the wing upper surface flow structure and pressure distribution but has a minimal impact on the integrated upper surface pressure increments.

Introduction

Historically, aerodynamicists have designed aircraft for efficient supersonic flight by employing attached-flow wing design philosophy. A review of previous wing design studies shows that for cruise lift conditions, linearized theory methods (refs. 1 and 2) have produced efficient designs, and at high-lift conditions, full-potential methods (refs. 3 and 4) have been employed to obtain efficient attached-flow designs. However, attached-flow, high-lift wing geometries are typically characterized by large amounts of wing leading-edge camber and bluntness, which result in a large drag penalty at low lift typical of supersonic cruise conditions. (See ref. 5.) Attempts to employ variable camber devices to minimize the cruise performance penalty have met with limited success (ref. 6) because the resulting aerodynamic performance for variable camber designs at either cruise or high-lift conditions is typically degraded from the optimum fixed camber geometry. (See ref. 5.)

An alternate wing design philosophy for efficient supersonic flight employs a controlled leading-edge vortex system. Investigations at subsonic and transonic speeds of the wing employing this leading-edge vortex design philosophy have shown that significant performance benefits over a broad flight envelope may be obtained. Compared with the attached-flow designs, the advantages of the vortex-flow design concept are many: the wing surfaces of the variable camber devices are not as critical because flow separation is forced; the design requires a thin, sharp leading edge, which is more suitable for minimizing supersonic wave drag; and the supersonic design constraints are more consistent with those for subsonic and transonic vortex-flow designs.

To address this new design challenge at supersonic speeds, a research program was established in the early 1980's at the Langley Research Center to study wing leading-edge vortex flows at supersonic speeds. (See refs. 7 and 8.) As depicted in figure 1, even the most basic of wing leading-edge vortex systems (on a flat-top, uncambered delta wing) can be quite complex; and as the wing geometry becomes more complex (i.e., thickness, camber), the resulting vortex-flow structure would contain many additional flow features and with increasing Mach number, additional flow features would appear. The wing vortex-flow research at supersonic speeds was structured to take full advantage of the available experimental (ref. 9) as well as computational research capabilities at this Center. In addition, the simplicity of the wind tunnel model geometry lends itself well to computational studies. (See refs. 10 and 11.) The three major wing geometric parameters in the study are leading-edge sweep, camber, and airfoil shape and thickness. Shown in figure 2 are photographs of the zero-thick, cambered, and thick delta wing models installed in the Langley Unitary Plan Wind Tunnel (ref. 12). A zero-thick wing is represented by a wind tunnel model which is characterized by a flat upper surface and minimum thickness on the lower surface. The leading edges of the wing are sharp with a leading-edge bevel angle, measured normal to the wing leading edge, less than 10° and located entirely on the lower surface. The influences of wing leading-edge sweep and camber were documented previously in references 12 and 13, respectively, and the effect of the airfoil is documented in the present report.

Figures 3 and 4 show the resulting six types of flow fields identified for the zero-thick and cambered wings, respectively.

In addition to the flow classification effort for zero-thick and cambered wings, an extensive effort has been directed at understanding the vortex-induced aerodynamics for delta wings. A set of curves which represent the normal-force coefficients

of the upper and lower surfaces of the zero-thick and cambered delta wings has been generated by integrating experimentally obtained pressure distributions on the wing surface. (See fig. 5, which was taken from ref. 7.)

The present paper summarizes the previous results and compares them to recent results obtained for a series of eight uncambered delta-wing models which varied in leading-edge sweep and airfoil geometry.

Experimental Test

Model Description

Planform sketches of the thick delta wing wind tunnel models are shown in figure 6. The eight delta wing models consisted of a 7-percent-thick diamond airfoil and a 7-percent-thick circular-arc airfoil with leading-edge sweeps of 52.5°, 60°, 67.5°, and 75°. (See fig. 7.)

The leeward surface of each model was instrumented with a spanwise row of 19 pressure orifices evenly spaced and located 1 in. forward of the wing trailing edge. The 19 pressure orifices were located on both the left- and right-hand wing panels between 0 and 90 percent, in 10 percent increments, of the local wing semispan. Pressure data were obtained with a 48-port, electronic scanning pressure gauge system mounted outside the tunnel. Pressure data on the lower surface were obtained by rolling the model 180° and repeating the pitch sweep.

The models were connected to the tunnel permanent mounting system by a dogleg sting. A photograph of a typical assembly consisting of a model and sting is depicted in figure 8. The support arrangement was designed to minimize support interference effects on the pressure instrumented wing surface opposite the sting attachment point.

During the test, angle of attack was measured with an accelerometer located in the tunnel permanent model-actuating system. The measured angle of attack was corrected for tunnel flow angularity; no angle-of-attack corrections were required for deflections of the dogleg sting.

Test Conditions

Testing was conducted in the low Mach number test section of the Langley Unitary Plan Wind Tunnel, which is a variable Mach number, variable pressure, variable temperature, continuous-flow supersonic tunnel. The test section is 4 by 4 by 7 ft (ref. 9).

The tests were conducted at a sideslip angle of 0° and at angles of attack from 0° to 28° for the nominal set of conditions listed in the following table:

M	Total pressure, lb/ft^2	Total temperature, °F	Reynolds number per foot
1.70	1114	125	2×10^6
2.00	1254	125	2×10^6

The dew point was maintained at −20°F when pressure data were obtained to eliminate condensation effects.

To ensure fully turbulent boundary-layer flow over the model surface, boundary-layer transition strips composed of No. 60 sand grit were applied 0.2 in. behind the wing leading edges (measured normal to the leading edge). The transition strips were approximately 0.0625 in. wide.

Flow Visualization Techniques

In addition to the surface pressure data two types of flow visualization data were obtained. Vapor-screen photographs were taken to provide information on the flow field above the wing surface, and oil-flow photographs were used to examine the flow characteristics on the model surface. Model preparation prior to flow visualization tests consisted of painting one coat of flat black paint over a coat of zinc chromate primer. These three different types of tests were done sequentially.

Vapor-screen flow visualization data are obtained by passing a thin sheet of high-intensity light through a foglike condition in the tunnel test section. The fog is created in the tunnel test section by adding water in the diffuser downstream from the tunnel test section until a uniform fog was produced in the test section. The test conditions which provided the best fog quality for a Reynolds number per foot of 2×10^6 are given in the following table:

M	Total pressure, lb/ft^2	Total temperature, °F	Dew point, °F
1.70	1114	100	13
2.00	1254	117	19

The dew point was measured in the tunnel settling chamber and corrected to standard atmospheric conditions.

A high-intensity tungsten light source mounted outside the tunnel on the sidewall was used to produce a thin light sheet across the tunnel test section.

The light sheet was oriented perpendicular to the tunnel flow and positioned at the same streamwise location on the delta wings as the surface pressure taps. Photographs were taken by a camera mounted to the ceiling inside the tunnel and located approximately 3 ft downstream from the model. (See sketch A, which shows details of the vapor screen setup.)

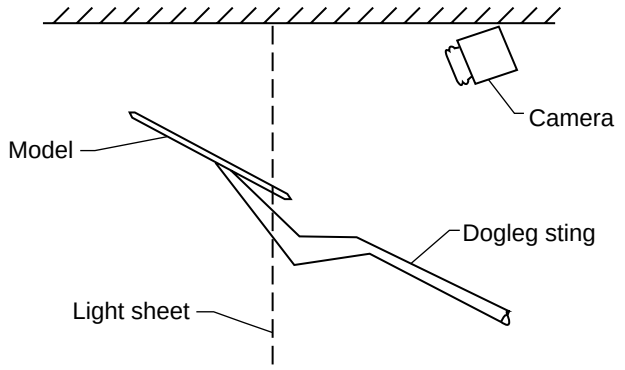

Sketch A

Oil-flow photographs required the same model-surface flat black painting as previously discussed. The model surface was then brushed with a mixture of 90W oil containing yellow fluorescent powder. Oil-flow photographs were taken through the test-section door window by two cameras mounted outside the tunnel. The model was rolled 90° and was illuminated by four ultraviolet lamps mounted outside the tunnel. During the tunnel start-up period, the model was kept in a wings-horizontal position to keep as much oil on the wing as possible. To obtain photographs, the model was rolled 90° (wings vertical) and angle of attack was set by yawing the model. After the model was positioned, approximately 3 to 4 min was required for the oil-flow pattern to stabilize. Normally, only 3 or 4 different angles of attack could be documented before the oil had to be replaced. Photographs were obtained at angles of attack of 0°, 8°, and 16°.

Discussion of Experimental Results

The primary purpose of the present research is to assess the influence of airfoil geometry and flow conditions on wing leading-edge vortex flow at supersonic speeds.

The present thick-wing geometries do not reflect a particular design philosophy but have been developed to provide a large variation in flow conditions, based upon the previous work. To provide a reference for the thick wings, results for the previously tested four zero-thick flat delta wings are also presented in this section of the paper.

This section of the paper only addresses the critical elements of the research results; however, all the data for the thick delta wings are presented in appendixes A and B. Flow visualization data, oil flow and vapor screen, are contained in appendix A, and upper and lower surface pressure coefficient data are contained in appendix B.

Representative experimental results are presented in figures 9 through 14. Presented in figure 9 are oil-flow photographs showing the influence of airfoil shape on the wing upper surface flow for the 60° swept wing at a Mach number of 1.70 for angles of attack of approximately 0°, 8°, and 16°. At $\alpha \approx 0°$, the flow patterns for all wings show attached flow; however, the one for the diamond airfoil indicates that the flow is undergoing an abrupt expansion about the wing maximum thickness ridge line as evidenced by the surface flow in this region. This expansion on the wing upper surface for the diamond airfoil existed at all angles of attack and Mach numbers. The oil-flow photograph also indicates that a cross-flow recompression shock is beginning to form at the apex of the wing maximum thickness line for the diamond airfoil. The photographs for $\alpha \approx 8°$ clearly show that the addition of thickness delays the onset of leading-edge separation. The delay in leading-edge separation appears to be related to an angle of attack equivalent to one half the airfoil leading-edge included angle. At an angle of attack of approximately 16°, all wings show the influence of a leading-edge vortex with a secondary separation.

The influence of wing leading-edge sweep angle on the upper surface flow is shown in figure 10. The oil-flow photographs of figure 10 show that the flat and circular-arc wings have similar flow characteristics in that both show the conical flow structure and a wing leading-edge vortex structure. However, results for the diamond airfoil show that a significant change in the flow structure occurs aft of the airfoil maximum thickness ridge line. Comparing the data of figure 9 with that of figure 10 shows that the influence of wing airfoil shape increases significantly with increasing wing sweep. In particular, the data for the 75° swept delta wing with the diamond airfoil at $\alpha \approx 8°$ appear to show that the wing leading-edge vortex, whose presence is indicated by the oil accumulation line lying near the leading edge and emanating from the apex, disappears aft of the airfoil maximum thickness line. Aft of the airfoil maximum thickness line there is a thick oil accumulation line which emanates from the apex of the airfoil maximum thickness line. This type of pattern in an oil flow is indicative of a cross-flow recompression shock (ref. 5). Because of the increased influence of the airfoil on the delta-wing

lee-side flow structure with increasing wing leading-edge sweep, the rest of the paper focuses on the 75° wing.

To assess the influence of the airfoil on upper surface loading, plots of spanwise surface pressure distributions are presented for the 75° wings at $M = 2.00$ for angles of attack of approximately 0°, 8°, and 16° in figures 11, 12, and 13, respectively. In addition to the surface pressure data, computer-enhanced photographs (CEP) of the vapor-screen flow visualization data are presented in each figure.

Spanwise surface pressure data and CEP vapor-screen flow visualization data are presented in figure 11 for the diamond, circular-arc, and flat 75° swept delta wings at $M = 2.00$ and $\alpha \approx 0°$. The CEP data of figure 11 clearly show that a cross-flow shock does exist on the lee side of the wing with the diamond airfoil (see dark region above the wing) and is located at a semispan position η of approximately 0.7. The surface pressure data show that the flat and circular-arc airfoils have very benign pressure distributions compared with the diamond airfoil which exhibits a significant pressure rise due to the cross-flow shock at a value of η between 0.650 and 0.725. Note that this is well inboard of the location of the airfoil maximum thickness ridge line which is located at $\eta = 0.95$ for this streamwise position. Another observation in the data of figure 11 is the existence of large negative surface pressure coefficients in the inboard region for the circular-arc wing compared with either the diamond or flat wing. These low pressures are undoubtedly due to the expansion of the flow over the wing maximum thickness line. Despite this expansion of the flow for the circular-arc wing, the resultant flow characteristics are very similar to those observed for the flat wing. It should be noted that the pressure data presented are for a streamwise position of 95 percent of the total wing length. The pressure forward of the airfoil maximum thickness line would be positive for the diamond and circular-arc wings at $\alpha \approx 0°$.

Presented in figure 12 are spanwise surface pressure distributions and vapor-screen CEP's of the 75° delta wings at $M = 2.00$ and $\alpha \approx 8°$ ($M_N = 0.58$, $\alpha_N = 28.5$). The data show that a leading-edge vortex has formed on all wings, as indicated in the photographs by the dark elliptic- or circular-shape regions located near the wing surface and emanating from the wing leading edge. A close examination of the flow visualization data shows that the vortex-flow structures for the three wings are considerably different. The flat-wing flow is characterized by a classical leading-edge vortex with a secondary vortex located below and outboard of the primary vortex. This is what would be expected for the conditions of $M_N = 0.58$ and $\alpha_N = 28.5$. (See fig. 3.) Vapor-screen photographs for both the diamond and circular-arc airfoil wings show a less pronounced vortex structure which lies very close to the wing surface and which appears to be more like a wing leading-edge bubble than a classical leading-edge vortex. If the value of α_N is corrected for the wing-surface streamwise angle, as was done for the cambered wing of figure 4, the α_N values for the diamond and circular-arc wings would become 20° and 12°, respectively. A review of figure 4 indicates that for a delta wing with the circular-arc airfoil at $M_N = 0.58$ and $\alpha_N = 12°$, a leading-edge bubble would be expected, and for the diamond airfoil $M_N = 0.58$ and $\alpha_N = 20°$, a leading-edge vortex would occur. The only other flow structure present for either wing is a cross-flow shock, which was observed to lie on top of the vortex for the diamond airfoil wing. Based upon the flow classification chart of figure 4 and the data for the circular-arc and flat wings under investigation, it may be concluded that this shock structure is a result of the local wing-surface contour of the diamond airfoil wing and not a function of the free-stream Mach number or angle of attack. For the diamond airfoil wing at these conditions, the vortex with shock structure would only occur on the aft portion of the wing behind the airfoil maximum thickness ridge line. Forward of the ridge line, the flow is characterized by a leading-edge vortex only; inboard of the vortex, the flow reattaches and flows streamwise. (See fig. 1.) As this streamwise flow passes over the ridge line, the flow expands and then recompresses resulting in a shock structure which sweeps aft and outboard. At approximately three fourths of the wing length, the wing leading-edge vortex and the ridge line shock intersect, as shown in figure 10, and the resulting flow structure is formed.

A review of the surface pressure data in figure 12 shows that all wings experience low pressure near the leading edge due to the separated flow; however, as observed in the data at $\alpha \approx 0°$ of figure 11, the recompression of the flow for the three wings varies significantly. At $\alpha \approx 8°$, the circular-arc wing experiences the least recompression of the wings and, as a result, has lower pressures inboard of the vortex compared with those of the diamond and flat wings. Despite these differences, the change in wing upper surface loading, as determined by integrating the pressure distribution from the $\alpha = 0°$ condition for each wing, is very similar.

At an angle of attack of $\approx 16°$, the flow structures and resultant lee-side pressure distributions for the three wings become similar. Presented in

figure 13 are surface pressure distributions and vapor-screen CEP's for the 75° wings at $M = 2.00$ and $\alpha \approx 16°$. The spanwise surface pressure coefficients become quite similar and are characterized by a low-pressure plateau region outboard and a gradual recompression. Again, the dominant influence of the airfoil on the pressures is observed in the level of the wing centerline pressure value.

A review of the vapor-screen photographs in figure 13 shows that all three wings have similar structures which are characterized by a vortex with shock. Only the diamond airfoil wing has a second shock structure which appears to lie both above and below the vortex feed sheet. This structure can again be attributed to the expansion about the airfoil ridge line.

The preceding analysis showed that the flow classification and aerodynamics of thick wings are similar to that for flat wings. However, a remaining question concerning the analysis of the vortex flow is the location of the vortex both laterally and vertically above the wing. To assess this characteristic, the vapor-screen flow visualization data were used to determine vortex location as a function of angle of attack. A representative analysis is shown in figure 14 for the 75° swept wings at $M = 2.00$. As mentioned previously, the diamond and circular-arc airfoil delta wings experience a delay in the leading-edge separation due to the local wing leading-edge surface slope. The data presented in figure 14 show that the vortex migration for all wings follows a similar path. In general, the vortex will initially be located near the wing surface at the leading edge. With increasing angle of attack, the vortex will move upward and inboard. These data are of great importance to the designer because the location of the vortex coincides with the location of the wing upper surface suction pressures, and the management of these suction pressures is critical to the success of the separated flow wing design concept.

Concluding Remarks

A review of the Langley wing leading-edge vortex-flow research at supersonic speeds has been presented along with results from a recent experimental study in which the influence of wing airfoil shape on wing leading-edge vortex flow was assessed. The review of the program was presented to provide a reference in which to discuss the effects of airfoil shape on wing leading-edge vortex flows.

The analysis of the 7-percent-thick delta wing data indicated that both the lee-side flow classification and local wing loading are quite similar to that obtained on zero-thick flat wings. Detailed analysis of the flow visualization data show that the flow about the wings with a diamond airfoil is more complex than that about a smooth airfoil wing. The surface discontinuity at the airfoil maximum thickness line for the diamond airfoil produces shocks and large expansions which interact with the leading-edge vortex to create vortex shock and vortex with multiple shock flow types. Flow visualization data also show that the influence of the airfoil contour of the lee-side flow field is increased significantly with increasing wing leading-edge sweep. These complex flow features were observed to have a significant impact on the wing upper surface pressure distributions.

NASA Langley Research Center
Hampton, VA 23665-5225
January 15, 1992

References

1. Carlson, Harry W.; and Middleton, Wilbur D.: *A Numerical Method for the Design of Camber Surfaces of Supersonic Wings With Arbitrary Planforms.* NASA TN D-2341, 1964.

2. Carlson, Harry W.; and Miller, David S.: *Numerical Methods for the Design and Analysis of Wings at Supersonic Speeds.* NASA TN D-7713, 1974.

3. Siclari, Michael J.: *The NCOREL Computer Program for 3D Nonlinear Supersonic Potential Flow Computations.* NASA CR-3694, 1983.

4. Shankar, Vijaya; Szema, Kuo-Yen; and Bonner, Ellwood: *Full Potential Methods for Analysis/Design of Complex Aerospace Configurations.* NASA CR-3982, 1986.

5. Miller, David S.; Pittman, Jimmy L.; and Wood, Richard M.: An Overview of Two Nonlinear Supersonic Wing Design Studies. AIAA-83-0182, Jan. 1983.

6. Covell, Peter F.; Miller, David S.; and Wood, Richard M.: An Evaluation of Leading-Edge Flap Performance on Delta and Double-Delta Wings at Supersonic Speeds. AIAA-86-0315, Jan. 1986.

7. Wood, Richard M.; and Miller, David S.: Assessment of Preliminary Prediction Techniques for Wing Leading-Edge Vortex Flows at Supersonic Speeds. AIAA-84-2208, Aug. 1984.

8. Miller, David S.; and Wood, Richard M.: An Investigation of Wing Leading-Edge Vortices at Supersonic Speeds. AIAA-83-1816, July 1983.

9. Jackson, Charlie M., Jr.; Corlett, William A.; and Monta, William J.: *Description and Calibration of the Langley Unitary Plan Wind Tunnel.* NASA TP-1905, 1981.

10. Murman, Earll M.; Powell, Kenneth G.; Miller, David S.; and Wood, Richard M.: Comparison of Computations and Experimental Data for Leading Edge Vortices—Effects of Yaw and Vortex Flaps. AIAA-86-0439, Jan. 1986.

11. Powell, Kenneth G.; and Murman, Earll M.: A Comparison of Experimental and Numerical Results for Delta Wings With Vortex Flaps. *A Collection of Technical Papers—AIAA 4th Applied Aerodynamics Conference,* June 1986, pp. 411–424. (Available as AIAA-86-1840.)

12. Miller, David S.; and Wood, Richard M.: *Lee-Side Flow Over Delta Wings at Supersonic Speeds.* NASA TP-2430, 1985.

13. Wood, Richard M.; and Watson, Carolyn B.: *Study of Lee-Side Flows Over Conically Cambered Delta Wings at Supersonic Speeds.* NASA TP-2660, Pts. 1 and 2, 1987.

Appendix A

Flow Visualization Photographs

Oil-flow photographs for the 75°, 67.5°, 60°, and 52.5° thick delta wing models are presented in figures A1, A2, A3, and A4, respectively, over the test range of Mach number and angle of attack. Vapor-screen photographs for the same models are presented in figures A5 through A20.

Appendix B

Surface Pressure Coefficient Data

Surface pressure coefficient data for the 75°, 67.5°, 60°, and 52.5° swept thick delta wing wind tunnel models are presented in tables B1 and B2, B3 and B4, B5 and B6, and B7 and B8, respectively.

REPORT DOCUMENTATION PAGE

Form Approved
OMB No. 0704-0188

1. AGENCY USE ONLY *(Leave blank)*	2. REPORT DATE	3. REPORT TYPE AND DATES COVERED
	March 1992	Technical Paper

4. TITLE AND SUBTITLE
Influence of Airfoil Geometry on Delta Wing Leading-Edge Vortices and Vortex-Induced Aerodynamics at Supersonic Speeds

5. FUNDING NUMBERS
WU 505-61-71-01

6. AUTHOR(S)
Richard M. Wood, James E. Byrd, and Gary F. Wesselmann

7. PERFORMING ORGANIZATION NAME(S) AND ADDRESS(ES)
NASA Langley Research Center
Hampton, VA 23665-5225

8. PERFORMING ORGANIZATION REPORT NUMBER
L-16851

9. SPONSORING/MONITORING AGENCY NAME(S) AND ADDRESS(ES)
National Aeronautics and Space Administration
Washington, DC 20546-0001

10. SPONSORING/MONITORING AGENCY REPORT NUMBER
NASA TP-3105

11. SUPPLEMENTARY NOTES
Wood: Langley Research Center, Hampton, VA; Byrd: Lockheed Engineering & Sciences Company, Hampton, VA; Wesselmann: On special assignment from Arnold Engineering Development Center, Arnold Air Force Base, TN.

12a. DISTRIBUTION/AVAILABILITY STATEMENT
Unclassified–Unlimited

Subject Category 02

12b. DISTRIBUTION CODE

13. ABSTRACT *(Maximum 200 words)*

An assessment of the influence of airfoil geometry on delta wing leading-edge vortex flows and vortex-induced aerodynamics at supersonic speeds is discussed. A series of delta wing wind tunnel models were tested in the Langley Unitary Plan Wind Tunnel over a Mach number range from 1.70 to 2.00. The model geometric variables included leading-edge sweep and airfoil shape. Surface pressure data and vapor-screen and oil-flow photographs were taken to evaluate the complex structure of the vortices and shocks on the family of wings tested. The data show that airfoil shape has a significant impact on the wing upper surface flow structure and pressure distribution but has a minimal impact on the integrated upper surface pressure increments.

14. SUBJECT TERMS
Supersonic aerodynamics; Delta wings; Vortex flows; Experimental

15. NUMBER OF PAGES
82

16. PRICE CODE
A05

17. SECURITY CLASSIFICATION OF REPORT	18. SECURITY CLASSIFICATION OF THIS PAGE	19. SECURITY CLASSIFICATION OF ABSTRACT	20. LIMITATION OF ABSTRACT
Unclassified	Unclassified		